

## ORIGINAL ARTICLE

# Altered neurite morphology and cholinergic function of induced pluripotent stem cell-derived neurons from a patient with Kleefstra syndrome and autism

J Nagy<sup>1,4</sup>, J Kobilák<sup>2,4</sup>, S Berzsényi<sup>1</sup>, Z Ábrahám<sup>1</sup>, HX Avci<sup>2,5</sup>, I Bock<sup>2</sup>, Z Bekes<sup>1</sup>, B Hodoscsek<sup>1</sup>, A Chandrasekaran<sup>2</sup>, A Téglási<sup>2</sup>, P Dezső<sup>1</sup>, B Koványi<sup>1</sup>, ET Vörös<sup>1</sup>, L Fodor<sup>1</sup>, T Szél<sup>1</sup>, K Németh<sup>3</sup>, A Balázs<sup>3</sup>, A Dinnyés<sup>2</sup>, B Lendvai<sup>1</sup>, G Lévy<sup>1</sup> and V Román<sup>1</sup>

The aim of the present study was to establish an *in vitro* Kleefstra syndrome (KS) disease model using the human induced pluripotent stem cell (hiPSC) technology. Previously, an autism spectrum disorder (ASD) patient with Kleefstra syndrome (KS-ASD) carrying a deleterious premature termination codon mutation in the *EHMT1* gene was identified. Patient specific hiPSCs generated from peripheral blood mononuclear cells of the KS-ASD patient were differentiated into post-mitotic cortical neurons. Lower levels of *EHMT1* mRNA as well as protein expression were confirmed in these cells. Morphological analysis on neuronal cells differentiated from the KS-ASD patient-derived hiPSC clones showed significantly shorter neurites and reduced arborization compared to cells generated from healthy controls. Moreover, density of dendritic protrusions of neuronal cells derived from KS-ASD hiPSCs was lower than that of control cells. Synaptic connections and spontaneous neuronal activity measured by live cell calcium imaging could be detected after 5 weeks of differentiation, when KS-ASD cells exhibited higher sensitivity of calcium responses to acetylcholine stimulation indicating a lower nicotinic cholinergic tone at baseline condition in KS-ASD cells. In addition, gene expression profiling of differentiated neuronal cells from the KS-ASD patient revealed higher expression of proliferation-related genes and lower mRNA levels of genes involved in neuronal maturation and migration. Our data demonstrate anomalous neuronal morphology, functional activity and gene expression in KS-ASD patient-specific hiPSC-derived neuronal cultures, which offers an *in vitro* system that contributes to a better understanding of KS and potentially other neurodevelopmental disorders including ASD.

Translational Psychiatry (2017) 7, e1179; doi:10.1038/tp.2017.144; published online 25 July 2017

## INTRODUCTION

Reprogramming of somatic cells into induced pluripotent stem cells is a powerful new approach that makes previously impracticable *in vitro* disease modeling possible in the case of many human diseases. This statement is especially true for central nervous system disorders including Alzheimer's disease, amyotrophic lateral sclerosis, Parkinson's disease, schizophrenia and autism spectrum disorder.<sup>1</sup> With respect to autism spectrum disorder (ASD), there is a limited, nevertheless growing number of studies on both non-syndromic<sup>2–5</sup> and syndromic forms of the disease.<sup>6</sup> Investigations using the human induced pluripotent stem cell (hiPSC) technique to model homogenous populations of syndromic autism with well-known, monogenic backgrounds have been done in Fragile X, Rett, Phelan-McDermid and Timothy syndromes.<sup>7–11</sup> These studies revealed that hiPSC-derived neuronal cultures could recapitulate some of the cellular phenotypes of the given syndrome, thus they were suggested to be valid disease models.<sup>12,13</sup>

Kleefstra syndrome (KS; OMIM 610253) is a rare genetic disorder with an estimated frequency of 1:200 000 that may present with a clinical phenotype including developmental delay, intellectual disability of a varying degree, childhood hypotonia, epilepsy/febrile seizures, distinctive facial features as well as anatomical

(cardiac, renal, urogenital) abnormalities.<sup>14,15</sup> Furthermore, a growing number (23–100%) of KS individuals with ASD is described, which can be largely attributable to improving ASD identification procedures.<sup>16,17</sup> In addition, brain white matter development may also be abnormal in Kleefstra patients suggestive of a disordered connectivity.<sup>18–20</sup> The syndrome is caused by haploinsufficiency of the euchromatic histone lysine methyltransferase 1 (*EHMT1*) gene with a likely complete penetrance. Mutations causing this disorder are micro-deletions of chromosome 9q34.3 in 75–85% of the subjects; the remaining cases carry various heterozygous intragenic *EHMT1* variants.<sup>15,21</sup> This histone methyltransferase catalyzes mono (H3K9me1) and dimethylation (H3K9me2) at Lys-9 position of histone H3,<sup>22</sup> thereby it epigenetically regulates gene expression through chromatin remodeling and seems to play an important role in neurodevelopment.<sup>23–25</sup>

Previously, we reported a KS case with a *de novo* single-nucleotide variant (SNV) resulting in a premature termination codon in the *EHMT1* gene.<sup>16</sup> The patient was also diagnosed with ASD, however, the *de novo* *EHMT1* SNV, could not explain the autistic phenotype of further family members.<sup>16</sup> In order to study the effect of the pathogenic *EHMT1* mutation on neurodevelopment, in the present study we set out to establish a patient-derived (hiPSC) neuronal culture model of KS. To this end,

<sup>1</sup>Pharmacology and Drug Safety Research, Gedeon Richter Plc., Budapest, Hungary; <sup>2</sup>BioTalentum Ltd., Gödöllő, Hungary and <sup>3</sup>Autism Foundation, Budapest, Hungary. Correspondence: Dr J Nagy, Laboratory of Molecular Cell Biology, Gedeon Richter Plc. Gyömrői út 19-21., Budapest 1103, Hungary. E-mail: jozsef.nagy@richter.hu

<sup>4</sup>These authors contributed equally to this work.

<sup>5</sup>Current address: Universitäts-Hals-Nasen-Ohren-Klinik, Tuebingen, Germany.

Received 27 April 2017; accepted 28 April 2017

peripheral mononuclear blood cells (PMBCs) of the patient and two unrelated control subjects were utilized to produce hiPSC clones.<sup>26</sup> Since many ASD and KS symptoms are related to forebrain cortical function<sup>27</sup> and glutamatergic neurons are instrumental to correct functioning of the cortex,<sup>28</sup> hiPSCs were differentiated into functionally active forebrain cortical glutamatergic cells by employing a dual SMAD inhibition protocol.<sup>29–31</sup> Neuronal development was assessed by investigating neurite morphology and dendritic protrusions as well as functional activity of the neuronal cells. By extrapolating results from this single case, this *in vitro* system may shed light on basic underlying mechanisms of brain developmental abnormalities in KS and potentially other neurodevelopmental disorders including idiopathic ASD.

## MATERIALS AND METHODS

### Subject characterization

Detailed characterization of the KS-ASD patient was reported previously.<sup>16</sup> Briefly, the female KS-ASD subject (aged 12 years at the time of blood sampling) was selected from the clinical sample of the Autism Foundation's Outpatient Clinic, Budapest, Hungary. The study was approved by the Research-Ethics Committee of Heim Pál Childrens' Hospital (permission number KUT-83/2013). Written informed consent had been obtained from the legal guardians before the subject entered the study. In agreement with the common KS clinical phenotype, the subject was characterized by developmental delay, childhood hypotonia, behavioral and psychiatric disorders as well as various facial features, while epilepsy or intellectual disability could not be identified. The child met diagnostic criteria of autism spectrum disorder (DSM-IV-TR;<sup>32,33</sup> and Autism Diagnostic Interview Revised (ADI-R)<sup>34</sup>). Detailed diagnostic results were previously published in detail.<sup>16</sup> In short, the KS-ASD subject was found moderately ill; social functions, stereotyped and adaptive behaviors were moderately affected while communication and daily functioning showed only mild impairments. ADI-R social, communication and repetitive behaviors diagnostic scores for were 12, 17 and 4, respectively. The patient was diagnosed with a *de novo* premature termination codon (PTC) resulting in haploinsufficient *EHMT1* gene expression and presented characteristic symptoms of KS.<sup>16</sup> Two unrelated healthy control subjects (CTL1 and CTL2) were used as controls with negative autism diagnosis based on the assessment of ADOS and ADI-R. The two controls were both young adults,<sup>35</sup> Caucasians and represented both the male and female sex.

### hiPSC derivation and neural differentiation

hiPSCs were obtained by reprogramming PMBCs of the subjects with a non-integrative method as described previously.<sup>26</sup> In addition to the previously established two hiPSC lines from the KS-ASD patient (KS-ASD S2, S4), two hiPSC lines from each control (CTL1 S11, S16 and CTL2 S5, S9) were also generated, selected and characterised with similar methodology, as in the case of the KS-ASD patient. Full characterization (pluripotency, differentiation into the three germ layers, absence of Sendai-virus expression as well as karyotyping) of a KS-ASD patient-derived hiPSC line was published previously.<sup>26</sup> All hiPSC lines were maintained on matrigel (BD Biosciences, San Jose, CA, USA) in mTESR1 (Stemcell Technologies, Vancouver, BC, Canada) culture medium. To obtain neural progenitor cells (NPCs) mTESR1 medium was replaced with neuronal induction medium (NIM) (1:1 mixture of DMEM/F12 and Neurobasal medium supplemented with 1% Penicillin/Streptomycin, 1% NEAA, 1% N2, 2% B27, 100  $\mu$ M 2-ME, 1% glutamine; all from Thermo Fisher Scientific (Waltham, MA, USA), supplemented with 5 ng/ml bFGF (Thermo Fisher Scientific) on a confluent hiPSC plate (one well of a 6-well plate). After one day of culturing, cells were passaged 1:1 with Accutase (3 min) and plated onto poly-L-ornithine (Sigma-Aldrich, St. Louis, MO, USA) and laminin (Roche Diagnostics, Mannheim, Germany) (POL/L) coated dishes in NIM medium supplemented with 5  $\mu$ g ml<sup>-1</sup> insulin (Sigma-Aldrich), 500 ng ml<sup>-1</sup> Noggin (R&D Systems, Minneapolis, MN, USA) and 10  $\mu$ M SB431542 (Sigma-Aldrich). To increase cell viability, 10  $\mu$ M Rock Inhibitor (Y27632; Sigma-Aldrich) was also added to the medium for the first 24 h. Fresh culture medium was given to the cells daily for 9 days, then the formed neuroepithelial cell layer was dissociated with Trypsin-EDTA solution (Sigma-Aldrich) and cells were replated into laminin coated dishes in NIM medium supplemented with 10 ng ml<sup>-1</sup> bFGF and 10 ng ml<sup>-1</sup> EGF (Promokine, Heidelberg, Germany).

After 5–7 days, the formed neuronal rosettes were picked manually and were further cultured. After characterization of the obtained NPCs, cells were frozen in a medium containing 10% dimethyl sulfoxide and 90% FBS (Sigma-Aldrich) and were stored in liquid nitrogen until used. For generation of post-mitotic neural cells (forebrain glutamatergic neurons), NPCs were cultured in neural maintenance medium (NMM; 1:1 mixture of DMEM/F-12 and Neurobasal media supplemented with 1% N2, 2% B27, 1% NEAA, 1% Antibiotic Antimycotic Solution (Sigma-Aldrich), 25  $\mu$ M 2-ME) supplemented with 10 ng ml<sup>-1</sup> bFGF (Thermo Fisher Scientific) and 10 ng ml<sup>-1</sup> EGF on POL/L substrate. Upon confluence, the NPCs were seeded into POL/L-treated dishes containing neuronal differentiation medium (1:1 mixture of DMEM/F-12 and Neurobasal media, 1% N2, 2% B27, 1% NEAA, 1% Antibiotic Antimycotic Solution, 25  $\mu$ M 2-ME) supplemented with 10 ng ml<sup>-1</sup> BDNF (Promokine) and 10 ng ml<sup>-1</sup> GDNF (Promokine). Neuronal cells were maintained for up to 8 weeks with half medium change performed every 2–3 days. For neurite morphology, the cells were plated with 10 000 cells per cm<sup>2</sup>, while for other applications the cells were seeded with 20 000 cells per cm<sup>2</sup> cell density.

### Immunostaining and image analysis

Cells were fixed with 4% paraformaldehyde (PFA; Sigma-Aldrich) and were permeabilized with 0.2% Triton X 100 in PBS for 5 min then treated with blocking solution (BS; 2% BSA and 0.2% Triton X 100 in PBS) for 1 h at room temperature (RT). Samples were incubated with primary antibodies: anti-NESTIN antibody (Merck-Millipore, Billerica, MA, USA), anti-PAX6 antibody (BioLegend), anti-SOX1 antibody (R&D Systems), anti-MAP2, anti-Synapsin1, anti-NF200 antibodies (Abcam, Cambridge, UK), anti-TUJ antibody (Santa Cruz, Santa Cruz, CA, USA), anti-TAU antibody (Dako, Glostrup, Denmark), anti-vGLUT1/2 antibody (Synaptic Systems, Göttingen, Germany) in BS for 3 h (RT), then with secondary antibodies (Thermo Fisher Scientific) for 1.5 h. Nuclei were stained with DAPI (1  $\mu$ g ml<sup>-1</sup>, Sigma-Aldrich). For analysis of dendritic protrusions, high resolution confocal images were taken with an iMic confocal microscope (FEI, Hillsboro, OR, USA) using an oil immersion  $\times$ 60 objective. Segments connected to the neurites and longer than 1  $\mu$ m were defined as dendritic protrusions and were counted blindly in 40 pictures of each sample. Since abnormal dendritic development has been earlier reported in *EHMT1* knockout mice<sup>24</sup> and *Drosophila*,<sup>36</sup> gross neurite morphology was investigated. For analyzing neurite morphology, images were acquired with an Operetta high content screening system (PerkinElmer, Waltham, MA, USA) using  $\times$ 40 magnification. Image acquisition was carried out with a Harmony 3.5 software (Waltham, MA, USA) using excitation/emission filters of 380–445 nm and 630/705 nm for DAPI and MAP2/A633, respectively. First, cell nuclei were determined in the DAPI channel, then MAP2-positive cells were selected and analyzed for neurite morphology using the neurite tracing algorithm (CSIRO Neurite Analysis 2 formula of Harmony 3.5.2 Find Neurite plug-in; CSIRO Data61, Epping, VIC, Australia). Segments thicker than 2  $\mu$ m, longer than 25  $\mu$ m and connected to the soma were quantified. Neurite parameters were calculated from a minimum of 180 fields of view per samples. Data from at least three independent biological replicates from each cell line were collected, pooled by subjects and compared in pairs (KS-ASD vs CTL1 or CTL2) for statistical significance applying Mann–Whitney test. Graphs and error bars represent mean and S.E.M., respectively.

### Electron microscopy

Cells terminally differentiated for 5 weeks were fixed with a solution containing 3.2% PFA, 0.2% glutaraldehyde, 1% sucrose, 40 mM CaCl<sub>2</sub> in 0.1 M cacodylate buffer (Sigma-Aldrich) for 24 h at 4 °C. After rinsing for 2 days in cacodylate buffer, samples were post fixed in 1% ferrocyanide-reduced osmium tetroxide (Sigma-Aldrich; White *et al.*, 1979) for 1 h (RT), treated with aqueous 1% uranyl-acetate (BDH Chemicals, Radnor, PA, USA) for 30 min, embedded in Spurr low viscosity epoxy resin medium (Sigma-Aldrich) and cured for 24 h at 80 °C. Ultrathin sections were stained with Reynolds's lead citrate (Sigma-Aldrich) for 2 min and were examined in JEM 1010 transmission electron microscope (JEOL, Tokyo, Japan) operating at 60 kV. Photographs were taken using a Morada 11 megapixel camera with ITEM software (Olympus, Tokyo, Japan).

### Western blotting

Extracts of cells terminally differentiated for 10 days were obtained by applying RIPA lysis buffer (50 mM Tris, pH 8.0; 150 mM NaCl, 1% NP-40, 0.1% SDS, 10% glycerol, 9.8 mM NaF and 1% protease inhibitor cocktail;

Merck-Millipore). Samples containing equal amounts of proteins (30 µg per lane) were subjected to SDS-PAGE (NuPAGE Novex Bis-Tris Gel; 4–12%; Thermo Fisher Scientific) and blotted onto PVDF membrane (Merck-Millipore). After blocking with 5% w/v non-fat dry milk powder in 0.1% Tween 20 (Sigma-Aldrich), membranes were probed with antibodies specific for the N-terminal of the EHMT1 protein (ab135487, Abcam) and for GAPDH as control (Sigma-Aldrich). Signals were visualized with horseradish peroxidase-coupled anti-rabbit IgG antibody (Santa Cruz Biotechnology, Dallas, TX, USA) using ECL Plus Western Blot Detection System (GE Healthcare Europe, Freiburg, Germany). Intensity values were calculated using Image Studio Lite 5.2 software (LI-COR Biotechnology, Bad Homburg, Germany). Western blot analysis was performed on at least three independent biological replicates.

### Electrophysiology

For whole-cell patch-clamp recordings, terminally differentiated hiPSC-derived 8-week-old neuronal cultures grown on POL/L-treated coverslips were transferred to a recording chamber and superfused with an extracellular solution (140 mM NaCl, 5 mM KCl, 2 mM CaCl<sub>2</sub>, 2 mM MgCl<sub>2</sub>, 5 mM HEPES, 5 mM HEPES-Na, 10 mM glucose; pH=7.35; 310 mOsm; Sigma-Aldrich) at RT. Patch electrodes (resistance 3.5–4.5 MΩ) filled with an intracellular solution (80 mM KCl, 50 mM KF, 31 mM KOH, 5.3 mM CaCl<sub>2</sub>, 2 mM MgCl<sub>2</sub>, 4 mM ATP-Na<sub>2</sub>, 10 mM HEPES, 10 mM EGTA; pH=7.25; 300 mOsm; Sigma-Aldrich) were used for detection of sodium and potassium currents evoked by 8 and 100 ms long rectangular step depolarizations from –80 mV to 0 mV holding potential, respectively. For recording and analysis, an Axopatch 200B amplifier and pClamp 9.0 software (Molecular Devices, Sunnyvale, CA, USA) were used. Whole-cell currents were filtered at 10 kHz and digitized at a sampling rate of 20 kHz (Digidata 1320A, Molecular Devices). To elicit GABA responses, 30 µM GABA (Sigma-Aldrich) was administered for 5 s, and low-pass filtered (1 kHz) currents were recorded at a holding potential of –80 mV. In current clamp mode currents were injected to keep the resting potential around –60 mV and current steps (increments: 20 pA, *n*=6, 500 ms) were applied to evoke action potentials. 1 µM tetrodotoxin (TTX; Latoxan, Portes-lès-Valence, France), 10 mM tetraethylammonium (TEA, Sigma-Aldrich) and 10 µM bicuculline (Sigma-Aldrich) were used to block sodium and potassium currents as well as GABA-evoked responses, respectively.

### Live cell calcium imaging

After 3, 5 or 8 weeks of terminal differentiation, hiPSC-derived neural cells were incubated with Calcium 6-QF indicator (Thermo Fisher Scientific) in Hank's balanced salt solution (HBSS: 137 mM NaCl, 5 mM KCl, 0.9 mM Mg<sub>2</sub>SO<sub>4</sub>, 1.4 mM CaCl<sub>2</sub>, 3 mM NaHCO<sub>3</sub>, 0.6 mM Na<sub>2</sub>HPO<sub>4</sub>, 0.4 mM KH<sub>2</sub>PO<sub>4</sub>, 20 mM HEPES, 5.6 mM glucose; pH 7.4; Sigma-Aldrich) for 2 h at 37 °C. Fluorescence intensity of the dye excited at 488 nm in cell somas was measured using an iMic fluorescence microscope (FEI) equipped with a 10×0.4 NA objective (Olympus) and a 1.4 megapixel cooled CCD camera (Andor Technologies, Belfast, UK) by taking pictures at a frame rate of 5.2 frames/sec. After 90 s recording—when spontaneous activity was monitored—cells were stimulated with acetylcholine (0.1 mM) dissolved in HEPES-buffered salt solution (140 mM NaCl, 5 mM KCl, 2 mM CaCl<sub>2</sub>, 1 mM MgCl<sub>2</sub>, 10 mM HEPES, 2 mM probenecid; pH 7.4; Sigma-Aldrich) and fluorescence intensity was recorded for a further 90 s. In case of glutamate (0.5 mM) stimulation, cells were incubated in presence of Fluo-4-AM calcium indicator (Thermo Fisher Scientific) in HBSS (45 min, at 37 °C) and fluorescent signals were recorded as described previously. Signals were recorded and analyzed using a Live Acquisition software (FEI).  $\Delta F/F_0$  values were calculated as the ratio of the change in fluorescent intensity evoked by the compounds ( $\Delta F$ ) and the baseline fluorescence ( $F_0$ ). The mean of the highest  $\Delta F/F_0$  values obtained during the 90-s observation period were collected from at least three biological replicates of KS-ASD and CTL1 cell lines, and were compared in pairs applying two-sample (Student's) *t*-test.

### Measurement of mRNA expression

Total RNA was isolated with High Pure RNA Isolation Kit (Roche Diagnostics) from neural cells after 10 days of differentiation. Quality control of the obtained samples and calculation of their RNA concentrations were accomplished using a Bioanalyzer 2100 with RNA 6000 Nano Assay II kits (Agilent Technologies, Santa Clara, CA, USA). RNA samples (1 µg each) were reverse transcribed with SuperScript VILO cDNA Synthesis Kit (Thermo Fisher Scientific). *EHMT1* transcript variant 1 and 2 were

determined using TaqMan Gene Expression Assays Hs00964329\_m1 and AIWR4AN, respectively (Thermo Fisher Scientific) with a LightCycler 2.0 real-time PCR (Roche Diagnostics). The positions of the primer pairs applied are shown in Supplementary Figure S3. To reveal differences in gene expression of neuronal cells from the KS-ASD and control subjects, 197 ASD-related genes were selected (Supplementary Table S1) and quantified using custom-made 384-well TaqMan low-density array cards (Thermo Fisher Scientific) and an ABI PRISM 7900HT real-time PCR system (Thermo Fisher Scientific). To functionally categorize these genes DAVID Bioinformatics Resources was implemented, by which the significantly overrepresented Gene Ontology (GO) and Kyoto Encyclopedia of Genes and Genomes (KEGG) categories were determined (Supplementary Table S1). Hits were validated in three biological replicates from each cell line using single TaqMan probes. Cycling conditions were used according to the manufacturer. Relative expression levels were calculated with the comparative C<sub>T</sub> method<sup>37</sup> and were normalized to the expression levels of the housekeeping genes *GAPDH*, *GUSB* and *HPRT1*. Mean mRNA levels of genes from KS-ASD patient-derived neural cells were compared to the levels obtained in case of the controls (CTL1 and CTL2). For statistical analysis, nonparametric Mann–Whitney test was used.

## RESULTS

### Neural differentiation of hiPSCs

Two hiPSC lines were established from PBMCs of the Kleefstra syndrome patient with autism (KS-ASD S2 and S4) using a non-integrative Sendai-virus (SeV) delivery system.<sup>26</sup> Likewise, control hiPSC lines—each from unrelated neurotypical subjects (CTL1 S11, S16 and CTL2 S5, S9)—were also generated to unveil the possible morphological and functional differences. Similarly to those of the KS-ASD hiPSC lines, pluripotent characteristics of the control hiPSC lines were verified by detection of pluripotency-associated marker proteins (OCT4, NANOG, E-CADHERIN) and by demonstration of their ability to spontaneously differentiate towards the 3 germ layers (Supplementary Figure S1). Neural precursor cells (NPCs) differentiated from hiPSCs of KS-ASD patient and both healthy controls expressed neural stem cell markers such as SOX1, PAX6 and NESTIN (Supplementary Figure S2). Terminally differentiated neurons on day 35 of differentiation were positive for the neuron-specific tubulin TUJ1, the microtubule-associated proteins MAP2 and TAU, as well as for the axonal Neurofilament-200 (NF200) and the glutamatergic subtype specific marker VGLUT1/2 (Figure 1). Overall, hiPSC-derived neuronal cells were successfully generated.

### Differentiated hiPSC-derived cells form active neuronal network in culture

Following 8 weeks of post-mitotic neural differentiation, hiPSC-derived neural cells expressed the presynaptic protein Synapsin1 (SYN1; Figure 2a). The presence of functional synapses was verified by electron microscopic studies showing synaptic clefts and vesicles in presynaptic terminals (Figure 2d). In agreement with these data, whole-cell patch-clamp recordings revealed depolarization-induced Na<sup>+</sup> and K<sup>+</sup> currents indicative of excitable cells. In addition, action potentials were also detected by current injection in a membrane potential-dependent manner. Furthermore, GABA application onto the cells was able to evoke currents supporting the observation that matured cells possessed several neuronal features (Figure 2b). The average current amplitudes and action potentials were not different in cells from the KS-ASD patient and the healthy controls. Average GABA response, Na<sup>+</sup> and K<sup>+</sup> currents in 9–22-day-old CTL vs KS-ASD neurons were 508 ± 111 (*n* = 22) vs 509 ± 113 pA (*n* = 27), 1053 ± 156 (*n* = 35) vs 994 ± 183 pA (*n* = 33) and 469 ± 58 (*n* = 39) vs 495 ± 69 pA (*n* = 35), respectively. The number of action potentials in 5-week-old CTL and KS-ASD neurons in response to 500 ms long 40 pA current injection were 3.1 ± 0.6 (*n* = 15) and 2.8 ± 0.8 (*n* = 9), respectively. Live-cell calcium imaging experiments revealed that spontaneous activity arose as early as 3 weeks of differentiation and the Ca<sup>2+</sup> transients

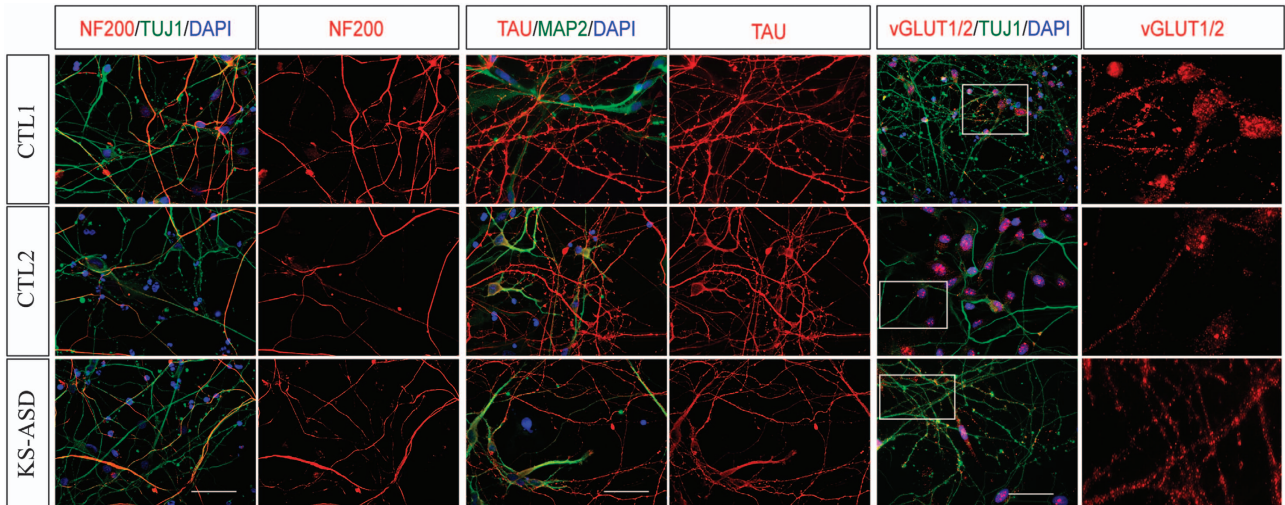


**Figure 1.** Neurons differentiated from human induced pluripotent stem cell (hiPSC)-derived neuronal precursor cells (NPCs). Representative images of CTL1, CTL2 and KS-ASD cells expressing the neuronal markers class III beta-tubulin (TUJ), Neurofilament 200 (NF200), and microtubule-associated proteins TAU and MAP2 on day 35 of terminal differentiation. The neurons are also positive for the glutamatergic subtype-specific marker vesicular neurotransmitter transporter 1/2 (vGLUT1/2). Insets highlight the magnified regions of cells immunolabeled for vGlut1/2. Nuclei are counterstained with DAPI. Scale bars = 50  $\mu$ m. KS-ASD, Autism spectrum disorder patient with Kleefstra syndrome.

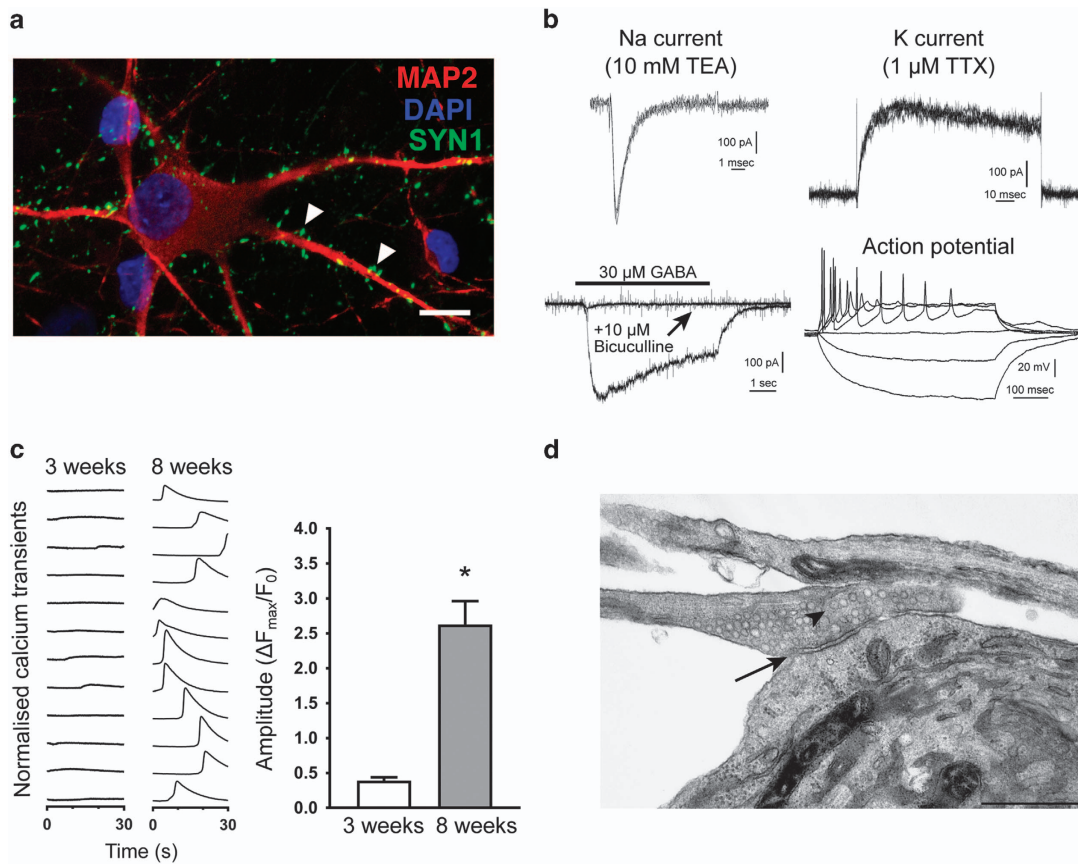


**Figure 2.** Physiologically active neurons differentiated from human induced pluripotent stem cell (hiPSC)-derived NPCs. (a) Expression of presynaptic protein Synapsin1 in MAP2-positive neuronal cells. Scale bar = 10  $\mu$ m. (b) Representative graphs of electrophysiological recordings of Na<sup>+</sup> and K<sup>+</sup> currents, Bicuculline-sensitive GABA-mediated response and evoked action potentials in 8-week-old hiPSC-derived CTL1 neurons. (c) Spontaneous calcium oscillations are more apparent in 8-week-old neurons than in 3-week-old neuronal cultures. Left, representative Ca<sup>2+</sup>-transients of individual neurons; right, quantification of Ca<sup>2+</sup>-transients 3 and 8 weeks after terminal differentiation. *t*-test, \**P* < 0.0001. (d) Presence of synaptic cleft (arrow) and presynaptic vesicles (arrowhead) was verified by electron microscope imaging in 5-week-old hiPSC-derived neurons. Scale bar = 500 nm.

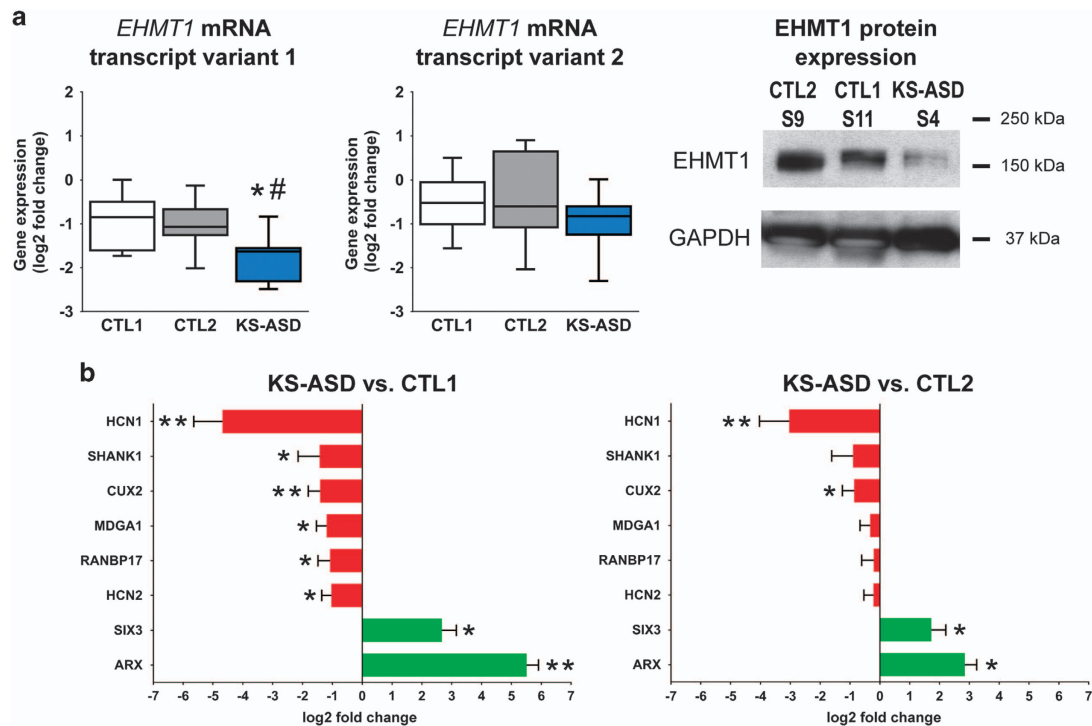


**Figure 3.** Reduced *EHMT1* mRNA expression and altered gene expression in human induced pluripotent stem cell (hiPSC)-derived neuronal cells from KS-ASD patient on day 10 of terminal differentiation. **(a)** The mRNA level of *EHMT1* transcript variant 1 is reduced in KS-ASD cells compared to CTL1 and CTL2 cells, whereas no change in the level of *EHMT1* transcript variant 2 is observed in KS-ASD vs control cells. *t*-test, CTL1 vs KS-ASD  $*P = 0.0061$ ; CTL2 vs KS-ASD  $^{\#}P = 0.0111$ . Right panel, Western blot analysis of *EHMT1* protein expression in CTL1, CTL2 and KS-ASD neurons. GAPDH was used as protein-loading control. **(b)** Gene expression changes in KS-ASD neurons compared to CTL1 (left) or CTL2 (right) neuronal cells on day 10 of terminal differentiation. Mann–Whitney test,  $*P < 0.05$ ,  $**P < 0.005$ .

became much more robust in 8-week-old cultured cells (Figure 2c). These results indicate that hiPSC-derived cortical neurons form functional networks in both control and KS-ASD lines.

#### Gene expression profiling of KS-ASD and control cells

Recently, a *de novo* mutation resulting in a premature termination codon (Trp1138Ter) in the euchromatic histone lysine methyltransferase 1 gene (*EHMT1*) of a KS-ASD patient was identified by targeted next-generation sequencing (NGS).<sup>16</sup> This mutation was shown to cause KS confirmed by the presence of a disorder-specific phenotype in the KS-ASD patient. Since the Trp1138Ter mutation possibly elicits nonsense-mediated mRNA decay causing decreased expression of *EHMT1*, we tested whether this mechanism was present in hiPSC-derived neuronal cells after 10 days of differentiation. We confirmed that mRNA level of the *EHMT1* transcript variant 1 (NM\_024757.4)—the variant carrying the mutation—was significantly lower in neuronal cells from the KS-ASD patient compared to both of the healthy controls (Figure 3a). In contrast, expression of *EHMT1* transcript variant 2 (NM\_001145527.1)—a shorter variant, not affected by the mutation—was the same in all samples (schematic structures of the *EHMT1* gene variants and positions of the primer pairs applied are shown in Supplementary Figure S3). In addition, western blot analysis revealed reduced *EHMT1* protein level in the KS-ASD cells, further supporting the presumption of an impaired *EHMT1* expression (Figure 3a).

Since *EHMT1* is known to be involved in epigenetic regulation of gene expression, we looked for possible alterations in gene expression profiles of KS-ASD patient-derived hiPSC neural cells. Altogether 197 target genes were selected from the SFARI database<sup>38</sup> (Gene Scoring Module category  $\leq 4$ ) and from the literature based on their relevance to ASD. Using DAVID

Bioinformatics Resources, we could evaluate the various Gene Ontology (GO) and Kyoto Encyclopedia of Genes and Genomes (KEGG) categories that the gene set encompassed. Based on the analysis, we ended up with a broad coverage of pathways related to development and function of the nervous system (Supplementary Table S1). The mRNA levels of the gene set were measured in hiPSC-derived neural cells of the KS-ASD patient and controls following 10 days of differentiation (Supplementary Table S1 and Supplementary Figure S5). *SIX3* and *ARX* homeobox genes involved in neural progenitor cell proliferation have been found to be upregulated in the neuronal cells derived from the KS-ASD patient (Figure 3b). *CUX2*, a homeobox gene related to neural specification, *SHANK1*, a gene involved in the structural and functional organization of dendritic spines and synaptic junctions, *MDGA1*, a gene important for neuronal migration, and *HCN1* and *HCN2*, genes regulating firing properties of the neurons were downregulated in the patient-derived neurons. In conclusion, disease-specific expression of ASD-related genes could be observed in the KS-ASD neuronal cultures.

#### Impaired neurite development in hiPSC-derived neurons of KS-ASD patient

To further investigate the effect of *EHMT1* haploinsufficiency on neural development, the hiPSC lines from the KS-ASD patient (KS-ASD clones S2 and S4) and from the neurotypical CTL1 (CTL1 clones S11 and S16) and CTL2 (CTL2 clones S5 and S9) subjects were terminally differentiated for 10 days, and immunostained for the neuronal marker MAP2. Morphology of the labeled cells was evaluated using an automated image analysis method quantifying the following parameters: number of MAP2-positive cells (neuronal cell number); total length of all neurites (total neurite length); length of the longest neurite of each cell (maximum neurite

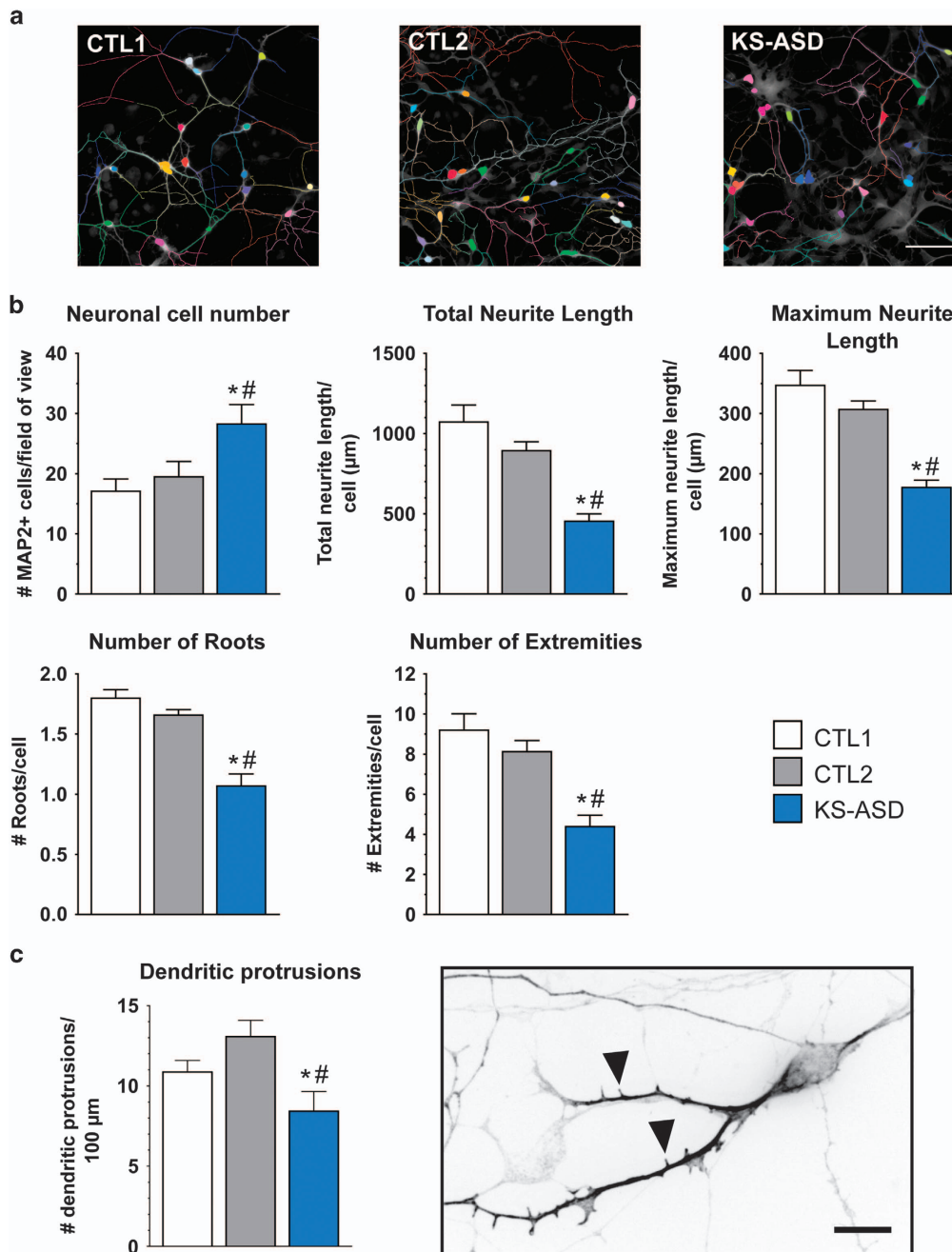


**Figure 4.** Impaired neurite morphology of hiPSC-derived neuronal cells from KS-ASD patient. (a) Neurite tracing of the neuronal cells labeled for MAP2 on day 10 of terminal differentiation. Scale bar = 50 μm. (b) Quantification of the number of MAP2-positive neuronal cells and parameters of neurite morphology of cells from KS-ASD and controls on day 10 of terminal differentiation. The results of the measurements are presented as mean data set of the two cell lines per KS-ASD, CTL1 and CTL2. Mann–Whitney test, \* $P < 0.05$  in KS-ASD vs CTL1, # $P < 0.05$  in KS-ASD vs CTL2. (c) Graph representing decreased number of dendritic protrusions on neuronal cells from KS-ASD patient on day 14 of terminal differentiation. Mann–Whitney test, \* $P < 0.05$  in KS-ASD vs CTL1, # $P < 0.05$  in KS-ASD vs CTL2. Arrowheads on the photograph point to dendritic protrusions. Scale bar = 10 μm.

length); number of neurites grown out of the cell body (number of roots); and number of the ends of all the neurites of a cell (number of extremities; Figure 4a). The results of the measurements are presented as means of the data obtained from two cell lines per person. As it is shown in Figure 4b, significantly more MAP2-labeled cells were found in the KS-ASD cultures than in the controls. On the other hand, KS-ASD-derived neuronal cells had significantly fewer roots and shorter neurites with fewer branches compared to both controls (Figure 4b). In case of the KS-ASD patient and CTL2 subject, there were no differences in these

parameters when the individual cell lines of each subject were compared (KS-ASD S2 vs S4 and CTL2 S5 vs S9), but one of the CTL1 cell lines (CTL1 S11) had significantly longer neurites with more abundant arborization compared to CTL1 S16 (Supplementary Figure S4). This variation in morphology of the CTL1 cell lines made KS-ASD more distinct from CTL1 than from CTL2.

Since the dendritic spine is a crucial component of chemical synapses and therefore imperative for interneuronal communication, we analyzed the number and length of developing protrusions

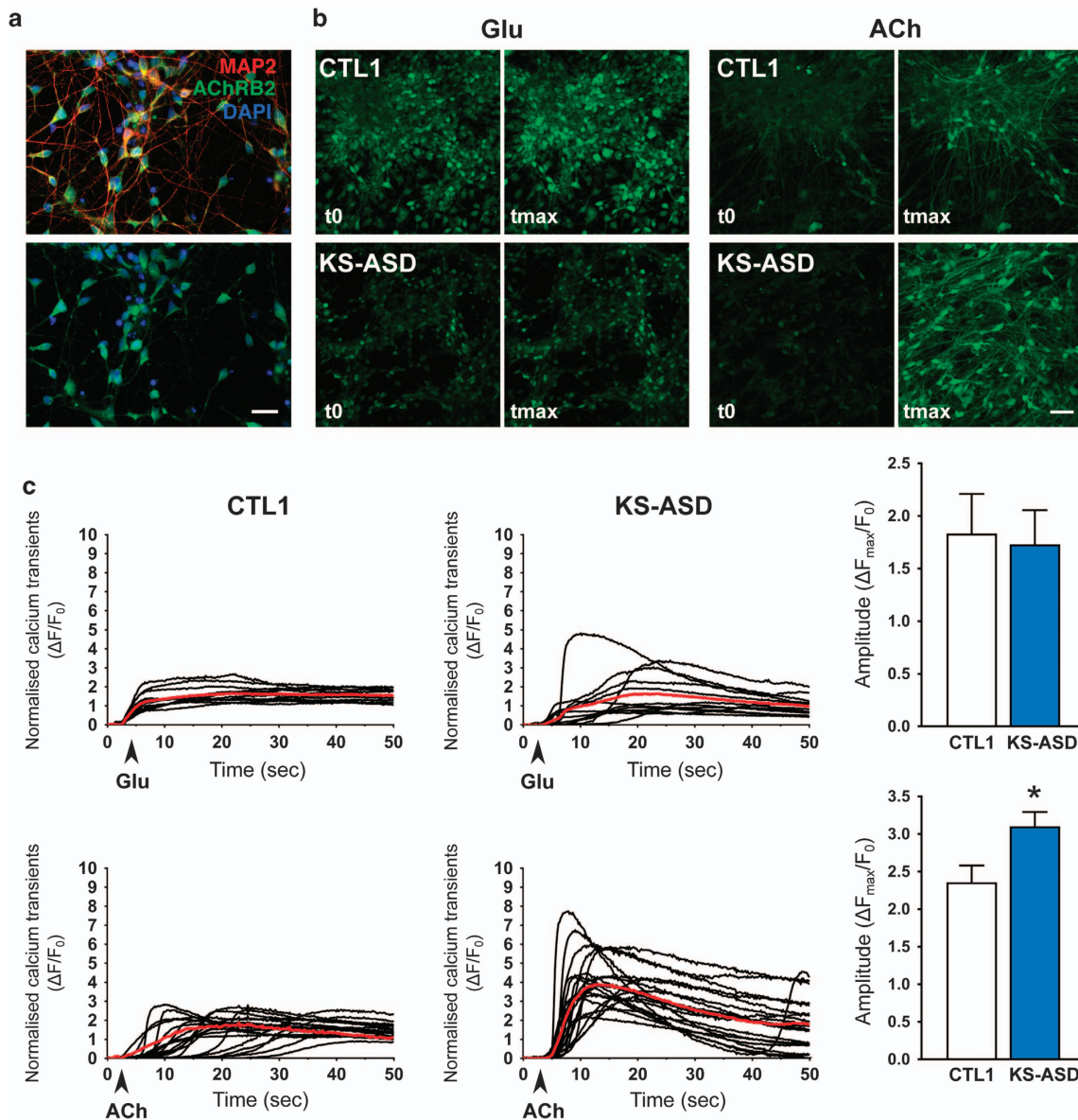


**Figure 5.** Increased acetylcholine-evoked calcium signal in neuronal cells differentiated from KS-ASD patient-derived hiPSCs. **(a)** Expression of Nicotinic Acetylcholine Receptor beta 2 (AChRB2, green) in MAP2-positive 4-week-old hiPSC-derived neurons. Scale bar = 20  $\mu$ m. **(b)** Change in fluorescence intensity upon administration of glutamate (Glu) or acetylcholine (ACh) onto 8-week-old control (CTL1) and KS-ASD neurons pre-loaded with Calcium 6-QF dye. Scale bar = 50  $\mu$ m. **(c)** Representative graphs showing Glu and ACh-evoked Ca<sup>2+</sup>-responses in CTL1 and KS-ASD neurons. Right panels, quantification of the Ca<sup>2+</sup>-responses as the mean of maximal intensity of the responses after treating the cells with Glu (upper) or ACh (lower). *t*-test, \**P* < 0.05. KS-ASD, Autism spectrum disorder patient with Kleefstra syndrome.

on neurites after 10 days of differentiation. While the mean length of protrusions did not differ significantly, density of protrusions was significantly lower in the KS-ASD samples compared to the controls (Figure 4c). In conclusion, KS-ASD-derived neurons displayed increased proliferation and impaired neurite morphology.

#### Altered calcium transients in hiPSC-derived neurons of KS-ASD patient

To understand whether hiPSC-derived neuronal cells express functional ionotropic receptors, neurotransmitter induced functional responses were examined at the single-cell level using fluorescence calcium imaging techniques. Topical application of glutamate and acetylcholine evoked calcium transients in almost 40% of the cells after 8 weeks of differentiation (Figure 5b). To

compare functional activity of neuronal cells from KS-ASD and control samples, calcium signals of at least 20, randomly chosen responding cells from each sample were plotted and were analyzed for the maximal fluorescence intensity (Figure 5). While glutamate-evoked responses were similar in neuronal cells from the KS-ASD and the CTL1 control samples, acetylcholine evoked significantly higher responses in KS-ASD patient-derived neuronal cells compared to CTL neurons (Figure 5c). In the latter case, calcium transients were reduced to 12 ± 2% (CTL1) and 16 ± 6% (KS-ASD) of the maximal response by the nicotinic acetylcholine receptor (nAChR) antagonist mecamylamine demonstrating that the calcium transients were evoked due to nAChR activation. From these results we can conclude that KS-ASD hiPSC-derived neurons are more sensitive to cholinergic pulses.

## DISCUSSION

ASD pathogenesis is yet to be resolved nevertheless, an attractive explanation for the disease is the atypical development of brain connectivity.<sup>39</sup> Supporting this idea, it is quite well documented in the literature that there is a maldevelopment of both long- and short-range connections in the autistic brain. Some examples of this abnormal long-range connectivity development include the thinning of the corpus callosum, the internal capsule, the fornices as well as the cerebellar white matter.<sup>40–43</sup> Local connectivity problems have also been identified in idiopathic ASD and neurodevelopmental syndromes as well as in various ASD mouse models.<sup>44</sup> Connectivity problems are not only present in idiopathic autism, but also in KS and its animal models.<sup>18,24,36</sup> Our results on the impaired neurite morphology in KS-ASD hiPSC-derived neuronal cultures are in agreement with the above structural findings of dendritic development in animal models. Furthermore, the morphological findings may also imply that white matter abnormalities in KS (such as corpus callosum agenesis or hypoplasia, periventricular leukomalacia, white matter reduction as well as generalized atrophy) could emerge from early malformation of interneuronal connections. Since similar morphological abnormalities have been described in hiPSC-based *in vitro* models of Fragile X syndrome<sup>7,45,46</sup> and idiopathic ASD,<sup>2</sup> compromised local and/or global connectivity patterns may very well be a shared underlying pathophysiological aspect of non-syndromic forms of ASD as well as associated neurodevelopmental disorders such as Fragile X syndrome.

One important hotspot of neural connectivity is the dendritic spine where most excitatory inputs make synaptic contacts. Defective pruning or initial overproduction of dendritic spines also contributes to local misconnectivity and synaptopathology in ASD.<sup>47</sup> Postmortem studies in human autism cases show that neocortical dendritic spine density is increased compared to neurotypicals.<sup>48</sup> In contrast, reduced spine density was observed in hiPSC-derived neurons of patients with Rett syndrome.<sup>49</sup> Although there is no anatomical evidence of impaired dendritic spine development in KS, *EHMT1* heterozygous knockout mice have significantly reduced numbers of mature spines on hippocampal CA1 pyramidal neurons.<sup>24</sup> Reduced numbers of mature spines is paralleled by increased numbers of primordial dendritic protrusions that have been found in various animal models of ASD and human postmortem brains.<sup>44</sup> Thus, it seems that decreased number of dendritic filopodia may be a general feature of ASD reflected in its *in vivo* models, also captured on the neurites of our KS-ASD patient-derived neurons.

Underdeveloped neurite morphology and the reduced number of dendritic protrusions were also accompanied by altered functional activity of the cultured neurons. Functional properties of hiPSC-derived neurons were thoroughly investigated recently using several different methods (e.g., patch-clamp recording, calcium flux) to demonstrate the presence of various ion channels (e.g., sodium, potassium and calcium voltage-gated channels) and receptors (e.g., AMPA, NMDA, GABA and ACh) in these cells.<sup>8,50–55</sup> In this study, we showed that neuronal cells indeed expressed functional ion channels and receptors both in control and KS-ASD cells. In addition, after 7 weeks of differentiation, generation of spontaneous neuronal activity was detected in each sample reflecting the emergence of mature synapses between neurons.<sup>8,54,56,57</sup> KS-ASD and control samples were identical in responding to glutamate challenge indicating the development of glutamatergic transmission was similar in the control and KS-ASD cultures. However, calcium signals following cholinergic pulses were higher in KS-ASD samples. This result suggests that development of the cholinergic system is impaired in the KS-ASD condition. Assuming that a higher cholinergic response reflects less acetylcholine because of the rapid desensitization of nicotinic receptors,<sup>58</sup> KS-ASD cultures might have a less

pronounced cholinergic transmission at baseline that corresponds well with the impaired morphology observed earlier in development. Corroborating this assumption, the nicotinic antagonist mecamylamine was able to block the response suggesting that nicotinic acetylcholine receptors (nAChRs) play a key role in creating the calcium response in these cells. The role for both nAChRs and muscarinic AChRs has been well defined in hippocampal synaptic plasticity.<sup>59,60</sup> It is also known that the timing of acetylcholine release and the subtype of receptor is critical for the type of plasticity induced.<sup>61</sup> Accordingly, the underdeveloped cholinergic transmission may entail some of the developmental deficits seen at the level of neurite morphology. Indeed, nAChRs can regulate the chloride transporter induction that is necessary for GABA to exert its central inhibitory role in neural networks.<sup>62</sup> It has also been shown that nAChRs contribute to the maturation of GABAergic synapses.<sup>63,64</sup> Therefore, some of the morphological impairments, especially the malformation of spine genesis in neurites, could be explained by a weaker cholinergic system in the KS-ASD cells. Nevertheless, this putative pathomechanism needs further confirmatory experiments.

Morphological abnormalities detected in the KS-ASD neurons are supported by mRNA expression patterns of ASD-associated genes: higher expression of proliferation-related genes and lower transcript level of genes involved in neuronal migration and maturation were found in the KS-ASD versus control neurons. Induction of genes involved in proliferation have been already reported in other *in vitro* hiPSC-derived systems including neuronal progenitors, neurons and cerebral organoids generated from non-syndromic ASD subjects.<sup>4,5</sup> While compromised neurite arborizations may be related to reduced expression of genes involved in maturation, the increased cell numbers in the KS-ASD cultures could be a consequence of increased expression of genes involved in proliferation. This latter finding is also of significance from a translational point of view, since in addition to the maldevelopment of white matter, an increased gray matter volume in most of the cerebral cortical regions is present during the first few years in children with autism.<sup>65</sup> This is most likely due to excessive proliferation as it was demonstrated in human postmortem studies<sup>66–69</sup> as well as in preclinical ASD<sup>70–73</sup> and KS models.<sup>74</sup>

Modeling of ASD and its related neurodevelopmental disorders is a great challenge of today's neuroscience. The paucity of postmortem autistic brains, the non-availability of *ex vivo* neuronal tissue and the limitations of preclinical *in vivo* models are all obstacles on the avenue leading to useful *in vitro* ASD models. A relatively novel approach to obtain such models is the reprogramming of patient-derived cells and their differentiation into neurons. In the present study, we produced neuronal cells from a KS patient along with two healthy controls. The neuronal cultures showed distinctive phenotypical features that were in line in many aspects with the theoretical foundations of ASD and KS including compromised neurite morphology and decreased number of dendritic protrusions. Potential mechanisms that may lead to such phenotype include altered cholinergic transmission and misregulation of genes involved in neuronal proliferation, maturation and migration. As recapitulation of disease phenotype is an expected hallmark of a disease model with reasonable translational power, the present hiPSC-derived neuronal cultures possessing such properties represent a useful *in vitro* system that serves a better understanding of Kleefstra syndrome and autism.

## CONFLICT OF INTEREST

JN, SB, ZA, ZB, BH, PD, BK, ETV, LF, TS, BL, GL and VR are full time employees of Gedeon Richter Plc. The remaining authors declare no conflict of interest.



## ACKNOWLEDGMENTS

We are grateful to the donating healthy subjects and the Kleefstra patient for their participation in our study. The present study was financially supported by Gedeon Richter Plc. and a Hungarian governmental grant (ERNYO-13-1-2013-000). Abinaya Chandrasekaran and Hasan X. Avci were financially supported by an EU FP7 Marie Curie Fellowship (EpiHealthNet, PITN-GA-2012-317146; and STEMMAD, PIAPP-GA-2012-324451). We thank Kinga Molnár, Lajos László and Mónika Truszka for their contribution in electron microscopy.

## AUTHOR CONTRIBUTIONS

JN, SB, BL, GL and VR conceived the study and wrote the manuscript. KN and AB diagnosed the patient and examined the healthy controls to prove being neurotypical with respect to ASD. JK and HXA performed experimental design, implemented the experiments, analyzed the data and participated in the interpretation of the results. IB identified the *EHMT1* mutation and participated in gene expression studies; AC and AT performed hiPSC culture and characterization, NPC generation and characterization; performed terminal differentiation of the samples for HCl. ZA, ZB and SB performed immunostainings and HCl measurements; ETV executed Western blots; BH counted dendritic protrusions and did calcium live cell imaging. PD and BK performed the gene expression studies. LF and TS recorded electrophysiology. AD conceived the study, read and approved the paper. All authors read and approved the final version of the paper.

## REFERENCES

- Corti S, Faravelli I, Cardano M, Conti L. Human pluripotent stem cells as tools for neurodegenerative and neurodevelopmental disease modeling and drug discovery. *Expert Opin Drug Discovery* 2015; **10**: 615–629.
- Griesi-Oliveira K, Acab A, Gupta AR, Sunaga DY, Chailangkarn T, Nicol X *et al*. Modeling non-syndromic autism and the impact of TRPC6 disruption in human neurons. *Mol Psychiatry* 2015; **20**: 1350–1365.
- Liu X, Campanac E, Cheung H-H, Ziats MN, Canterel-Thouennon L, Raygada M *et al*. Idiopathic autism: cellular and molecular phenotypes in pluripotent stem cell-derived neurons. *Mol Neurobiol* 2016.
- Marchetto MC, Belinson H, Tian Y, Freitas BC, Fu C, Vadodaria KC *et al*. Altered proliferation and networks in neural cells derived from idiopathic autistic individuals. *Mol Psychiatry* 2017; **22**: 820–835.
- Mariani J, Coppola G, Zhang P, Abyzov A, Provini L, Tomasini L *et al*. FOXG1-dependent dysregulation of GABA/glutamate neuron differentiation in autism spectrum disorders. *Cell* 2015; **162**: 375–390.
- Betancur C. Etiological heterogeneity in autism spectrum disorders: more than 100 genetic and genomic disorders and still counting. *Brain Res.* 2011; **1380**: 42–77.
- Doers ME, Musser MT, Nichol R, Berndt ER, Baker M, Gomez TM *et al*. iPSC-derived forebrain neurons from FXS individuals show defects in initial neurite outgrowth. *Stem Cells Dev* 2014; **23**: 1777–1787.
- Marchetto MCN, Carromeu C, Acab A, Yu D, Yeo GW, Mu Y *et al*. A model for neural development and treatment of Rett syndrome using human induced pluripotent stem cells. *Cell* 2010; **143**: 527–539.
- Pasca SP, Portmann T, Voineagu I, Yazawa M, Shcheglovitov A, Pasca AM *et al*. Using iPSC-derived neurons to uncover cellular phenotypes associated with Timothy syndrome. *Nat Med* 2011; **17**: 1657–1662.
- Shcheglovitov A, Shcheglovitova O, Yazawa M, Portmann T, Shu R, Sebastiano V *et al*. SHANK3 and IGF1 restore synaptic deficits in neurons from 22q13 deletion syndrome patients. *Nature* 2013; **503**: 267–271.
- Boland MJ, Nazor KL, Tran HT, Szücs A, Lynch CL, Paredes R *et al*. Molecular analyses of neurogenic defects in a human pluripotent stem cell model of fragile X syndrome. *Brain* 2017; **140**: 582–598.
- Acab A, Muotri AR. The use of induced pluripotent stem cell technology to advance autism research and treatment. *Neurotherapeutics* 2015; **12**: 534–545.
- Yu DX, Marchetto MC, Gage FH. Therapeutic translation of iPSCs for treating neurodegenerative disease. *Cell Stem Cell* 2013; **12**: 678–688.
- Kleefstra T, Brunner HG, Amiel J, Oudakker AR, Nillesen WM, Magee A *et al*. Loss-of-function mutations in euchromatin histone methyl transferase 1 (*EHMT1*) cause the 9q34 subtelomeric deletion syndrome. *Am J Hum Genet* 2006; **79**: 370–377.
- Kleefstra T, Nillesen WM, Yntema HG. *Kleefstra Syndrome*. In: Pagon RA, Adam MP, Ardinger HH, Wallace SE, Amemiya A, Bean LJH *et al*. (eds). *GeneReviews*: University of Washington, Seattle: Seattle, WA, USA, pp 1993–2017.
- Bock I, Nemeth K, Pentelenyi K, Balicza P, Balazs A, Molnar MJ *et al*. Targeted next generation sequencing of a panel of autism-related genes identifies an *EHMT1*

- mutation in a Kleefstra syndrome patient with autism and normal intellectual performance. *Gene* 2016; **595**: 131–141.
- Vermeulen K, de Boer A, Janzing JGE, Koelen DA, Ockeloen CW, Willemsen MH *et al*. Adaptive and maladaptive functioning in Kleefstra syndrome compared to other rare genetic disorders with intellectual disabilities. *Am J Med Genet A* 2017; **173**: 1821–1830.
- He X, Caluseriu O, Srivastava R, Denny AM, Bolduc FV. Reversible white matter lesions associated with mutant *EHMT1* and Kleefstra syndrome. *Neurol Genet* 2016; **2**: e58.
- Kleefstra T, van Zelst-Stams WA, Nillesen WM, Cormier-Daire V, Houge G, Foulds N *et al*. Further clinical and molecular delineation of the 9q subtelomeric deletion syndrome supports a major contribution of *EHMT1* haploinsufficiency to the core phenotype. *J Med Genet* 2009; **46**: 598–606.
- Verhoeven WMA, Egger JIM, Vermeulen K, van de Warrenburg BPC, Kleefstra T. Kleefstra syndrome in three adult patients: further delineation of the behavioral and neurological phenotype shows aspects of a neurodegenerative course. *Am J Med Genet A* 2011; **155A**: 2409–2415.
- Willemsen MH, Vulto-van Silfhout AT, Nillesen WM, Wissink-Lindhout WM, van Bokhoven H, Philip N *et al*. Update on Kleefstra syndrome. *Mol Syndromy* 2012; **2**: 202–212.
- Black JC, Van Rechem C, Whetstone JR. Histone lysine methylation dynamics: establishment, regulation, and biological impact. *Mol Cell* 2012; **48**: 491–507.
- Balemans MCM, Huibers MMH, Eikelenboom NWD, Kuipers AJ, van Summeren RCJ, Pijpers MMCA *et al*. Reduced exploration, increased anxiety, and altered social behavior: Autistic-like features of euchromatin histone methyltransferase 1 heterozygous knockout mice. *Behav Brain Res* 2010; **208**: 47–55.
- Balemans MCM, Kasri NN, Kopanitsa MV, Afinowi NO, Ramakers G, Peters TA *et al*. Hippocampal dysfunction in the Euchromatin histone methyltransferase 1 heterozygous knockout mouse model for Kleefstra syndrome. *Hum Mol Genet* 2013; **22**: 852–866.
- Kramer JM. Regulation of cell differentiation and function by the euchromatin histone methyltransferases G9a and GLP. *Biochem Cell Biol* 2016; **94**: 26–32.
- Varga E, Nemes C, Tancos Z, Bock I, Berzsenyi S, Levay G *et al*. Establishment of *EHMT1* mutant induced pluripotent stem cell (iPSC) line from a 11-year-old Kleefstra syndrome (KS) patient with autism and normal intellectual performance. *Stem Cell Res* 2016; **17**: 531–533.
- Barak B, Feng G. Neurobiology of social behavior abnormalities in autism and Williams syndrome. *Nat Neurosci* 2016; **19**: 647–655.
- Douglas RJ, Martin KAC. Neuronal circuits in the neocortex. *Annu Rev Neurosci* 2004; **27**: 419–451.
- Chambers SM, Fasano CA, Papapetrou EP, Tomishima M, Sadelain M, Studer L. Highly efficient neural conversion of human ES and iPSC cells by dual inhibition of SMAD signaling. *Nat Biotechnol* 2009; **27**: 275–280.
- Shi Y, Kirwan P, Smith J, Robinson HP, Livesey FJ. Human cerebral cortex development from pluripotent stem cells to functional excitatory synapses. *Nat Neurosci* 2012; **15**: 477–486, S1.
- Boissart C, Poulet A, Georges P, Darville H, Julita E, Delorme R *et al*. Differentiation from human pluripotent stem cells of cortical neurons of the superficial layers amenable to psychiatric disease modeling and high-throughput drug screening. *Transl Psychiatry* 2013; **20**: e294.
- American Psychiatric Association. *Diagnostic and Statistical Manual of Mental Disorders*; 4th edn (text rev.). American Psychiatric Association: Washington, DC, 2000.
- Lord C, Rutter M, DiLavore PC, Risi S. *Autism Diagnostic Observation Schedule*. Western Psychological Services: Los Angeles, CA, USA, 1999.
- Lord C, Rutter M, Le Couteur A. Autism Diagnostic Interview-Revised: a revised version of a diagnostic interview for caregivers of individuals with possible pervasive developmental disorders. *J Autism Dev Disord* 1994; **24**: 659–685.
- Mertens J, Apua CMP, Ku M, Hatch E, Böhnke L, Ladjevardi S *et al*. Directly reprogrammed human neurons retain aging-associated transcriptomic signatures and reveal age-related nucleocytoplasmic defects. *Cell Stem Cell* 2015; **17**: 705–718.
- Kramer JM, Kochinke K, Oortveld MAW, Marks H, Kramer D, de Jong EK *et al*. Epigenetic regulation of learning and memory by *Drosophila* *EHMT1/G9a*. *PLoS Biol* 2011; **9**: e1000569.
- Schmittgen TD, Livak KJ. Analyzing real-time PCR data by the comparative C (T) method. *Nat Protoc* 2008; **3**: 1101–1108.
- Abrahams BS, Arking DE, Campbell DB, Mefford HC, Morrow EM, Weiss LA *et al*. SFARI Gene 2.0: a community-driven knowledgebase for the autism spectrum disorders (ASDs). *Mol Autism* 2013; **4**: 36.
- Geschwind DH, Levitt P. Autism spectrum disorders: developmental disconnection syndromes. *Curr Opin Neurobiol* 2007; **17**: 103–111.
- Chung MK, Dalton KM, Alexander AL, Davidson RJ. Less white matter concentration in autism: 2D voxel-based morphometry. *Neuroimage* 2004; **23**: 242–251.

- 41 Courchesne E, Press GA, Yeung-Courchesne R. Parietal lobe abnormalities detected with MR in patients with infantile autism. *Am J Roentgen* 1993; **160**: 387–393.
- 42 McAlonan GM, Cheung V, Cheung C, Suckling J, Lam GY, Tai KS et al. Mapping the brain in autism. A voxel-based MRI study of volumetric differences and inter-correlations in autism. *Brain: J Neurol* 2005; **128**: 268–276.
- 43 Vidal CN, Nicolson R, DeVito TJ, Hayashi KM, Geaga JA, Drost DJ et al. Mapping corpus callosum deficits in autism: an index of aberrant cortical connectivity. *Biol Psychiatry* 2006; **60**: 218–225.
- 44 Martinez-Cerdeno V. Dendrite and spine modifications in autism and related neurodevelopmental disorders in patients and animal models. *Dev Neurobiol* 2017; **77**: 393–404.
- 45 Liu J, Koscielska KA, Cao Z, Hulsizer S, Grace N, Mitchell G et al. Signaling defects in iPSC-derived fragile X premutation neurons. *Hum Mol Genet* 2012; **21**: 3795–3805.
- 46 Sheridan SD, Theriault KM, Reis SA, Zhou F, Madison JM, Daheron L et al. Epigenetic characterization of the FMR1 gene and aberrant neurodevelopment in human induced pluripotent stem cell models of fragile X syndrome. *PLoS ONE* 2011; **6**: e26203.
- 47 Penzes P, Cahill ME, Jones KA, VanLeeuwen J-E, Woolfrey KM. Dendritic spine pathology in neuropsychiatric disorders. *Nat Neurosci* 2011; **14**: 285–293.
- 48 Hutsler JJ, Zhang H. Increased dendritic spine densities on cortical projection neurons in autism spectrum disorders. *Brain Res* 2010; **1309**: 83–94.
- 49 Kim K-Y, Hysolli E, Park I-H. Neuronal maturation defect in induced pluripotent stem cells from patients with Rett syndrome. *Proc Natl Acad Sci USA* 2011; **108**: 14169–14174.
- 50 Berry BJ, Akanda N, Smith AST, Long CJ, Schnepfer MT, Guo X et al. Morphological and functional characterization of human induced pluripotent stem cell-derived neurons (iCell Neurons) in defined culture systems. *Biotech Prog* 2015; **31**: 1613–1622.
- 51 Coyne L, Shan M, Przyborski SA, Hirakawa R, Halliwell RF. Neuropharmacological properties of neurons derived from human stem cells. *Neurochem Int* 2011; **59**: 404–412.
- 52 Dage JL, Colvin EM, Fouillet A, Langron E, Roell WC, Li J et al. Pharmacological characterisation of ligand- and voltage-gated ion channels expressed in human iPSC-derived forebrain neurons. *Psychopharmacology* 2014; **231**: 1105–1124.
- 53 Haythornthwaite A, Stoelzle S, Hasler A, Kiss A, Mosbacher J, George M et al. Characterizing human ion channels in induced pluripotent stem cell-derived neurons. *J Biomol Screen* 2012; **17**: 1264–1272.
- 54 Heikkilä TJ, Ylä-Outinen L, Tanskanen JMA, Lappalainen RS, Skottman H, Suuronen R et al. Human embryonic stem cell-derived neuronal cells form spontaneously active neuronal networks in vitro. *Exp Neurol* 2009; **218**: 109–116.
- 55 Weick JP, Liu Y, Zhang S-C. Human embryonic stem cell-derived neurons adopt and regulate the activity of an established neural network. *Proc Natl Acad Sci USA* 2011; **108**: 20189–20194.
- 56 Cao L, Tan L, Jiang T, Zhu X-C, Yu J-T. Induced pluripotent stem cells for disease modeling and drug discovery in neurodegenerative diseases. *Mol Neurobiol* 2015; **52**: 244–255.
- 57 Dravid SM, Murray TF. Spontaneous synchronized calcium oscillations in neocortical neurons in the presence of physiological [Mg(2+)]: involvement of AMPA/kainate and metabotropic glutamate receptors. *Brain Res* 2004; **1006**: 8–17.
- 58 Lendvai B, Kassai F, Szajli A, Nemethy Z. alpha7 nicotinic acetylcholine receptors and their role in cognition. *Brain Res Bull* 2013; **93**: 86–96.
- 59 Giocomo LM, Hasselmo ME. Neuromodulation by glutamate and acetylcholine can change circuit dynamics by regulating the relative influence of afferent input and excitatory feedback. *Mol Neurobiol* 2007; **36**: 184–200.
- 60 McKay BE, Placzek AN, Dani JA. Regulation of synaptic transmission and plasticity by neuronal nicotinic acetylcholine receptors. *Biochem Pharmacol* 2007; **74**: 1120–1133.
- 61 Gu Z, Yakel JL. Timing-dependent septal cholinergic induction of dynamic hippocampal synaptic plasticity. *Neuron* 2011; **71**: 155–165.
- 62 Liu Z, Neff RA, Berg DK. Sequential interplay of nicotinic and GABAergic signaling guides neuronal development. *Science* 2006; **314**: 1610–1613.
- 63 Kawai H, Zago W, Berg DK. Nicotinic alpha 7 receptor clusters on hippocampal GABAergic neurons: regulation by synaptic activity and neurotrophins. *J Neurosci* 2002; **22**: 7903–7912.
- 64 Zago WM, Massey KA, Berg DK. Nicotinic activity stabilizes convergence of nicotinic and GABAergic synapses on filopodia of hippocampal interneurons. *Mol Cell Neurosci* 2006; **31**: 549–559.
- 65 Schumann CM, Bloss CS, Barnes CC, Wideman GM, Carper RA, Akshoomoff N et al. Longitudinal magnetic resonance imaging study of cortical development through early childhood in autism. *JNeurosci* 2010; **30**: 4419–4427.
- 66 Courchesne E, Mouton PR, Calhoun ME, Semendeferi K, Ahrens-Barbeau C, Hallet MJ et al. Neuron number and size in prefrontal cortex of children with autism. *JAMA* 2011; **306**: 2001–2010.
- 67 Kotagiri P, Chance SA, Szele FG, Esiri MM. Subventricular zone cytoarchitecture changes in autism. *Dev Neurobiol* 2014; **74**: 25–41.
- 68 Pearson BL, Corley MJ, Vasconcellos A, Blanchard DC, Blanchard RJ. Heparan sulfate deficiency in autistic postmortem brain tissue from the subventricular zone of the lateral ventricles. *Behav Brain Res* 2013; **243**: 138–145.
- 69 Wegiel J, Kuchna I, Nowicki K, Imaki H, Wegiel J, Marchi E et al. The neuropathology of autism: defects of neurogenesis and neuronal migration, and dysplastic changes. *Acta Neuropathol (Berl)* 2010; **119**: 755–770.
- 70 Fang W-Q, Chen W-W, Jiang L, Liu K, Yung W-H, Fu AKY et al. Overproduction of upper-layer neurons in the neocortex leads to autism-like features in mice. *Cell Rep* 2014; **9**: 1635–1643.
- 71 Go HS, Kim KC, Choi CS, Jeon SJ, Kwon KJ, Han S-H et al. Prenatal exposure to valproic acid increases the neural progenitor cell pool and induces macrocephaly in rat brain via a mechanism involving the GSK-3beta/beta-catenin pathway. *Neuropharmacology* 2012; **63**: 1028–1041.
- 72 Pucilowska J, Vithayathil J, Tavares EJ, Kelly C, Karlo JC, Landreth GE. The 16p11.2 deletion mouse model of autism exhibits altered cortical progenitor proliferation and brain cytoarchitecture linked to the ERK MAPK pathway. *JNeurosci* 2015; **35**: 3190–3200.
- 73 Sabers A, Bertelsen FCB, Scheel-Kruger J, Nyengaard JR, Moller A. Long-term valproic acid exposure increases the number of neocortical neurons in the developing rat brain. A possible new animal model of autism. *Neurosci Lett* 2014; **580**: 12–16.
- 74 Benevento M, Oomen CA, Horner AE, Amiri H, Jacobs T, Pauwels C et al. Haploinsufficiency of EHMT1 improves pattern separation and increases hippocampal cell proliferation. *Sci Rep* 2017; **7**: 40284.



This work is licensed under a Creative Commons Attribution-NonCommercial-NoDerivs 4.0 International License. The images or other third party material in this article are included in the article's Creative Commons license, unless indicated otherwise in the credit line; if the material is not included under the Creative Commons license, users will need to obtain permission from the license holder to reproduce the material. To view a copy of this license, visit <http://creativecommons.org/licenses/by-nc-nd/4.0/>

© The Author(s) 2017

Supplementary Information accompanies the paper on the *Translational Psychiatry* website (<http://www.nature.com/tp>)